1 Mixing ratio computation

The constant term in equation (1) ($1.657\ 10^{-11}$) was calculated according to the PTRMS geometry and standard gas constants:

$$1.657\ 10^{-11} = \frac{\mu_0(cm^2\ V^{-1}\ s^{-1}) \times V_{mol\ air}^{std}(L\ mol^{-1}) \times {p_{air}^{std}}^2(mbar^2)}{{L_{drift}}^2(\ cm^2) \times N_A \times {T_{air}^{std}}^2(K^2)}$$

Where $\mu_0 = 2.8\ cm^2\ V^{-1}\ s^{-1}$ is reduced ion mobility in the drift, $V_{mol\ air}^{std} = 22400\ L\ mol^{-1}$ is the air molar volume in standard conditions, $p_{air}^{std} = 1013\ mbar$ is the standard pressure, $T_{air}^{std} = 273.15\ K$the standard temperature, $L_{drift} = 9.2\ cm$ the drift length, and $N_A = 6.022\ 10^{23}$the Avogadro number.

2 Calibration of the PTR-QI-TOF-MS

Table S1. Adjustment of the PTR-QI-TOF-MS toluene calibration factor with time. This adjustment was performed based on the 5 calibrations, the changes in E/N the 29/06/2016 and of the MCP detector before the 29/06. *S* is the calibration factor used in eq. (4) for all compounds except water vapour and methanol.

Date	E/N	MCP	$S_{toluene}$	Std. Err. on $S_{toluene}$	$\delta S_{toluene} / S_{toluene}$	R2
31/05/2016	150	2150	2.06	0.05	2.3%	1.00
13/06/2016	150	2200	2.47	0.07	3.0%	1.00
17/06/2016	150	2250	2.88	0.10	3.4%	1.00
23/06/2016	150	2300	3.29	0.13	3.8%	0.99
29/06/2016*	150	2300	3.29	0.13	3.8%	0.99
29/06/2016#	129	2300	3.49	0.12	3.4%	1.00
01/07/2016	129	2300	3.45	0.12	3.5%	1.00
07/07/2016	129	2300	3.28	0.11	3.4%	0.99
21/07/2016	129	2300	2.89	0.11	3.9%	0.99

30

Table S2. Calibration factors for individual compounds with respect to toluene $S / S_{toluene}$, and relative uncertainty on S.

Formula	m / z	$S / S_{toluene}$	Relative uncertainty on S (%)	Reference
NH3	18.034	10.011	15%	Koss et al. (2018)
C2H2	26.015	47.047	15%	Koss et al. (2018)
HCN	28.018	5.299	15%	Koss et al. (2018)
C2H4	28.031	91.176	15%	Koss et al. (2018)
CH3N	30.034	0.762	50%	Koss et al. (2018)
CH2O	31.018	8.705	15%	Koss et al. (2018)
CH4O	33.034	2.664	14%	This study
H2S	34.995	5.026	50%	Koss et al. (2018)
C2H3N	42.034	0.591	13%	This study
C3H6	43.054	3.127	50%	Koss et al. (2018)
HNCO	44.013	5.356	15%	Koss et al. (2018)
C2H5N	44.050	1.059	50%	Koss et al. (2018)
C2H4O	45.034	0.738	12%	This study
CH3NO	46.029	1.365	15%	Koss et al. (2018)
C2H7N	46.065	1.064	50%	Koss et al. (2018)
CH2O2	47.013	2.270	15%	Koss et al. (2018)
C2H6O	47.049	41.618	24%	This study
HNO2	48.008	186.867	15%	Koss et al. (2018)
CH4S	49.011	0.969	50%	Koss et al. (2018)
CH4O2	49.028	0.891	50%	Koss et al. (2018)
C3HN	52.018	0.507	50%	Koss et al. (2018)
C4H4	53.039	1.124	50%	Koss et al. (2018)
C3H3N	54.034	0.485	15%	Koss et al. (2018)
C3H2O	55.018	0.645	50%	Koss et al. (2018)
C4H6	55.054	1.222	50%	Koss et al. (2018)

Formula	m / z	S / $S_{toluene}$	Relative uncertainty on S (%)	Reference
C3H5N	56.050	0.542	50%	Koss et al. (2018)
C3H4O	57.034	1.447	11%	This study
C4H8	57.070	1.090	100%	Koss et al. (2018)
C2H3NO	58.029	1.722	15%	Koss et al. (2018)
C3H7N	58.065	1.047	50%	Koss et al. (2018)
C2H2O2	59.013	112.120	50%	Koss et al. (2018)
C3H6O	59.049	0.628	13%	This study
C2H5NO	60.044	1.379	15%	Koss et al. (2018)
C3H9N	60.081	1.138	50%	Koss et al. (2018)
C2H4O2	61.028	1.026	27%	Koss et al. (2018)
CH3NO2	62.024	1.213	15%	Koss et al. (2018)
C2H6S	63.026	0.950	50%	Koss et al. (2018)
C4H3N	66.034	0.505	50%	Koss et al. (2018)
C5H6	67.054	0.290	50%	Koss et al. (2018)
C4H5N	68.050	1.050	15%	Koss et al. (2018)
C3O2	68.997	0.846	100%	Koss et al. (2018)
C4H4O	69.034	1.080	15%	Koss et al. (2018)
C5H8	69.070	1.161	14%	This study
C4H7N	70.065	0.859	50%	Koss et al. (2018)
C3H2O2	71.013	1.053	50%	Koss et al. (2018)
C4H6O	71.049	0.881	12%	This study
C5H10	71.086	0.757	50%	Koss et al. (2018)
C4H9N	72.081	0.988	50%	Koss et al. (2018)
C3H4O2	73.028	0.944	50%	Koss et al. (2018)
C4H8O	73.065	0.680	15%	Koss et al. (2018)
C2H3NO2	74.024	0.533	50%	Koss et al. (2018)
C3H6O2	75.044	0.867	50%	Koss et al. (2018)
C2H5NO2	76.039	0.547	50%	Koss et al. (2018)
CH3NOS	78.001	1.055	100%	Koss et al. (2018)
C6H6	79.054	1.015	10%	This study
C5H5N	80.050	0.607	50%	Koss et al. (2018)
C5H4O	81.034	0.765	50%	Koss et al. (2018)
C5H7N	82.065	0.587	50%	Koss et al. (2018)
C5H6O	83.049	0.993	15%	Koss et al. (2018)
C5H9N	84.081	0.488	50%	Koss et al. (2018)
C4H4S	85.011	1.097	50%	Koss et al. (2018)
C4H4O2	85.028	0.792	50%	Koss et al. (2018)
C5H8O	85.065	0.754	50%	Koss et al. (2018)
C4H6O2	87.044	1.003	50%	Koss et al. (2018)
C5H10O	87.080	0.981	50%	Koss et al. (2018)
C3H4O3	89.023	0.725	50%	Koss et al. (2018)
C4H8O2	89.060	0.965	50%	Koss et al. (2018)
C3H7NO2	90.055	0.546	50%	Koss et al. (2018)
C6H5N	92.050	0.762	100%	Koss et al. (2018)
C7H8	93.070	1.000	11%	This study

Formula	m / z	S / $S_{toluene}$	Relative uncertainty on S (%)	Reference
C5H3NO	94.029	0.555	50%	Koss et al. (2018)
C6H7N	94.065	0.707	15%	Koss et al. (2018)
C2H6S2	94.998	0.769	100%	Koss et al. (2018)
C6H6O	95.049	1.274	15%	Koss et al. (2018)
C5H5NO	96.044	0.554	50%	Koss et al. (2018)
C6H9N	96.081	0.760	50%	Koss et al. (2018)
C5H4O2	97.028	0.642	15%	Koss et al. (2018)
C6H8O	97.065	1.005	50%	Koss et al. (2018)
C6H11N	98.096	0.491	50%	Koss et al. (2018)
C5H6S	99.026	0.984	50%	Koss et al. (2018)
C5H6O2	99.044	0.819	50%	Koss et al. (2018)
C6H10O	99.080	0.607	50%	Koss et al. (2018)
C4H4O3	101.023	0.718	50%	Koss et al. (2018)
C5H8O2	101.060	0.859	50%	Koss et al. (2018)
C6H12O	101.096	0.632	50%	Koss et al. (2018)
C4H6O3	103.039	0.655	100%	Koss et al. (2018)
C8H6	103.054	0.942	50%	Koss et al. (2018)
C7H5N	104.049	0.591	50%	Koss et al. (2018)
C8H8	105.070	0.870	15%	Koss et al. (2018)
C7H7N	106.065	0.737	50%	Koss et al. (2018)
C7H6O	107.049	0.690	50%	Koss et al. (2018)
C8H10	107.086	1.073	15%	Koss et al. (2018)
C6H5NO	108.044	0.744	100%	Koss et al. (2018)
C7H9N	108.081	0.626	15%	Koss et al. (2018)
C6H4O2	109.028	0.764	50%	Koss et al. (2018)
C7H8O	109.065	1.661	15%	Koss et al. (2018)
C7H11N	110.096	0.616	50%	Koss et al. (2018)
C6H6O2	111.044	1.166	15%	Koss et al. (2018)
C7H10O	111.080	0.896	50%	Koss et al. (2018)
C5H5NO2	112.039	0.545	50%	Koss et al. (2018)
C5H4O3	113.023	0.712	100%	Koss et al. (2018)
C6H8O2	113.060	0.798	50%	Koss et al. (2018)
C7H12O	113.096	0.612	50%	Koss et al. (2018)
C4H3NO3	114.019	0.766	100%	Koss et al. (2018)
C5H6O3	115.039	0.711	50%	Koss et al. (2018)
C6H10O2	115.075	0.805	50%	Koss et al. (2018)
C7H14O	115.112	0.620	50%	Koss et al. (2018)
C5H8O3	117.055	0.710	100%	Koss et al. (2018)
C9H8	117.070	0.886	50%	Koss et al. (2018)
C6H12O2	117.091	0.857	50%	Koss et al. (2018)
C4H7NO3	118.050	0.763	100%	Koss et al. (2018)
C8H7N	118.065	0.523	50%	Koss et al. (2018)
C8H6O	119.049	0.980	50%	Koss et al. (2018)
C9H10	119.086	0.889	50%	Koss et al. (2018)
C8H9N	120.081	0.724	50%	Koss et al. (2018)

Formula	m / z	S / $S_{toluene}$	Relative uncertainty on S (%)	Reference
C8H8O	121.065	0.610	50%	Koss et al. (2018)
C9H12	121.101	0.922	15%	Koss et al. (2018)
C7H6O2	123.044	0.613	50%	Koss et al. (2018)
C8H10O	123.080	0.845	50%	Koss et al. (2018)
C6H5NO2	124.039	0.947	15%	Koss et al. (2018)
C6H4O3	125.023	0.708	50%	Koss et al. (2018)
C7H8O2	125.060	0.989	15%	Koss et al. (2018)
C8H15N	126.128	0.480	50%	Koss et al. (2018)
C2H6S3	126.970	0.738	50%	Koss et al. (2018)
C6H6O3	127.039	0.707	50%	Koss et al. (2018)
C6H8O3	129.055	0.706	50%	Koss et al. (2018)
C10H8	129.070	0.876	50%	Koss et al. (2018)
C10H10	131.086	0.842	50%	Koss et al. (2018)
C9H9N	132.081	0.478	50%	Koss et al. (2018)
C9H8O	133.065	0.873	50%	Koss et al. (2018)
C10H12	133.101	0.837	50%	Koss et al. (2018)
C9H10O	135.080	0.607	50%	Koss et al. (2018)
C10H14	135.117	0.959	15%	Koss et al. (2018)
C8H8O2	137.060	0.833	100%	Koss et al. (2018)
C10H16	137.132	4.033	11%	This study
C7H7NO2	138.055	0.515	50%	Koss et al. (2018)
C8H10O2	139.075	0.989	15%	Koss et al. (2018)
C11H10	143.086	0.820	50%	Koss et al. (2018)
C6H8O4	145.050	0.692	100%	Koss et al. (2018)
C10H8O	145.065	0.840	50%	Koss et al. (2018)
C11H12	145.101	0.805	100%	Koss et al. (2018)
C10H10O	147.080	0.834	50%	Koss et al. (2018)
C10H12O	149.096	0.803	50%	Koss et al. (2018)
C11H16	149.132	0.795	50%	Koss et al. (2018)
C9H10O2	151.075	0.735	50%	Koss et al. (2018)
C8H8O3	153.055	1.412	15%	Koss et al. (2018)
C12H8	153.070	0.786	50%	Koss et al. (2018)
C10H16O	153.127	0.685	50%	Koss et al. (2018)
C8H10O3	155.070	0.694	50%	Koss et al. (2018)
C10H18O	155.143	0.790	100%	Koss et al. (2018)
C12H12	157.101	0.776	100%	Koss et al. (2018)
C10H20O	157.159	0.600	50%	Koss et al. (2018)
C12H18	163.148	0.763	50%	Koss et al. (2018)
C10H12O2	165.091	0.714	50%	Koss et al. (2018)
C13H20	177.164	0.735	50%	Koss et al. (2018)
C15H24	205.195	2.548	50%	Koss et al. (2018)

3 Compounds tentative identification and fluxes and mixing ratios summary

Table S3. VOC tentative identification and fluxes and mixing ratios summary

See file COV3ER_2016_dataset_summary.xlsx

4 Mixing ratio correlation analysis

Correlation between ions mixing ratios was found to be a power tool to identify possible fragments, and resolution issues. Table S4 shows the correlation coefficients over the periods with E/N = 130 and 150.

Table S4a. Ions for which 1h-averaged mixing ratio have a Pearson correlation coefficient larger than 0.9 over the entire experiment with E/N = 130

See file COV3ER_2016_dataset_summary.xlsx

Table S4b. Same as Table S4a with E/N = 150

See file COV3ER_2016_dataset_summary.xlsx

5 VOC eddy-covariance fluxes computation

In this section, the development of equation (6) is explained in details. This equation was derived by considering two issues: (1) the fact that the PTR- Qi-TOF- MS is measuring mixing ratio in wet air and not dry air, and (2) the fact that the cps is normalised by the primary ion source when calculating the mixing ratio in eq. (1).

5.1 Accounting for the contribution of water vapour in eddy-covariance fluxes computation with the PTR-Qi-TOF-MS

Eq. (5), which is reproduced below for clarity sake, is based on $\chi_{i,d}$, the mixing ratio in dry air of compound *i*:

$$F_i = \frac{\overline{p_a{}^d}}{R\overline{T_a}}\overline{w'\chi_{i,d}{}'} \quad \text{(S1)}$$

However, since the PTRMS measures a mixing ratio in wet air χ_i, its relation to $\chi_{i,d}$ needs to be accounted for:

$$\chi_{i,d} = \chi_i \times \frac{p_{drift}}{(p_{drift} - p_{v,drift})} \quad \text{(S2)}$$

Where $p_{v,drift}$ is the vapour pressure density in the drift. We also notice that:

$$\frac{p_{drift}}{p_{drift} - p_{v,drift}} = \left(1 + \chi_{v,drift,d}\right) \quad \text{(S3)}$$

Where $\chi_{v,drift,d}$ is the water vapour mixing ratio in dry air in the drift. Considering eqns. (S2) and (S3), yields:

$$\chi_{i,d} = \chi_i \times \left(1 + \chi_{v,drift,d}\right) \quad \text{(S4)}$$

Which can be differentiated to give:

$$\chi'_{i,d} = \chi'_i \times \left(1 + \chi_{v,drift,d}\right) + \chi_i \cdot \chi_{v,drift,d}{}' \quad \text{(S5)}$$

When injecting eq. (S5) in eq. (S1), one then gets the following expression for the flux:

$$F_i = \frac{\overline{p_a{}^d}}{R\overline{T_a}} \cdot \left[\left(1 + \overline{\chi_{v,drift,d}}\right) \cdot \overline{w'\chi'_i} + \overline{\chi_i} \cdot \overline{w'\chi'_{v,drift,d}}\right] \quad \text{(S6)}$$

Were $\overline{w'\chi'_{v,drift,d}}$ is the covariance of water vapour which can be expressed as a function of water vapour flux E (g m^{-2} s^{-1}):

$$w'\chi'_{v,drift,d} = \frac{E\,RT_a}{M_v p_a} \quad \text{(S7)}$$

where M_v is the water molar mass (g mol^{-1}). Assuming further that the drift water vapour pressure mixing ratio $\chi_{v,drift,d}$ is equal to the ambient one and equal to $\frac{p_{vap}}{p_a}$, one gets the following expression of the flux of compound χ_i:

$$F_i = \frac{\overline{p_a^d}}{R\overline{T_a}} \cdot \left(1 + \frac{p_{vap}}{p_a}\right) \cdot \overline{w'\chi_i'} + \frac{\overline{p_a^d}}{R\overline{T_a}} \cdot \overline{\chi_i} \cdot \frac{E\,RT_a}{M_v p_a} \quad \text{(S8)}$$

This hypothesis relies on the fact that the proportion of water vapour that is ionised is small, which is reasonable since a small fraction of water vapour is ionised. Finally, we can factorise $\overline{w'\chi_i'} \times \frac{\overline{p_a^d}}{R\overline{T_a}}$ in (S8) to yield the following expression:

$$F_i = \overline{w'\chi_i'} \times \frac{\overline{p_a^d}}{R\overline{T_a}} \times \left(1 + \frac{p_{vap}}{p_a} + \frac{1}{V_{exch,i}} \cdot \frac{E}{M_v}\frac{RT_a}{p_a}\right) \quad \text{(S9)}$$

Where $V_{exch,i}$ (in m s^{-1}) is the exchange velocity of compound *i* and is equal to $\overline{w'\chi_i'}/\overline{\chi_i}$. In this equation, the term p_{vap}/p_a accounts for dilution due to water vapour and the term on the right-hand side of the parenthesis accounts for correlated fluctuations of the water vapour mixing ratios in the drift tube. In practice, the correction terms were evaluated using the QCL water vapour measurements that were made in the same sampling tube and allowed to evaluate *E* and p_{vap}. This correction term will only be large for compounds with small exchange velocities $V_{exch,i}$, hence with small interest in terms of ecosystem exchange. Indeed, if we want this term to remain smaller than ε, we find that $V_{exch,i}$ should be larger than $ERT_a/(M_v p_a \varepsilon)$. Taking the maximum evaporation condition which is typically E ~ 0.2 g m^{-2} s^{-1}, and taking a maximum affordable ε = 0.25 we find that $V_{exch,i} > 0.1$ cm s^{-1}. For depositing compounds, this is a quite small deposition velocity. For emitting compounds, it depends on the atmospheric composition: compounds having large mixing ratios will lead to larger correction terms than those with low mixing ratios. On average, the correction term was found negligible over the campaign except for some compounds, which showed for a limited amount of time a correction larger than a few percent. These included noticeably acetone, for which the median correction was around 3%.

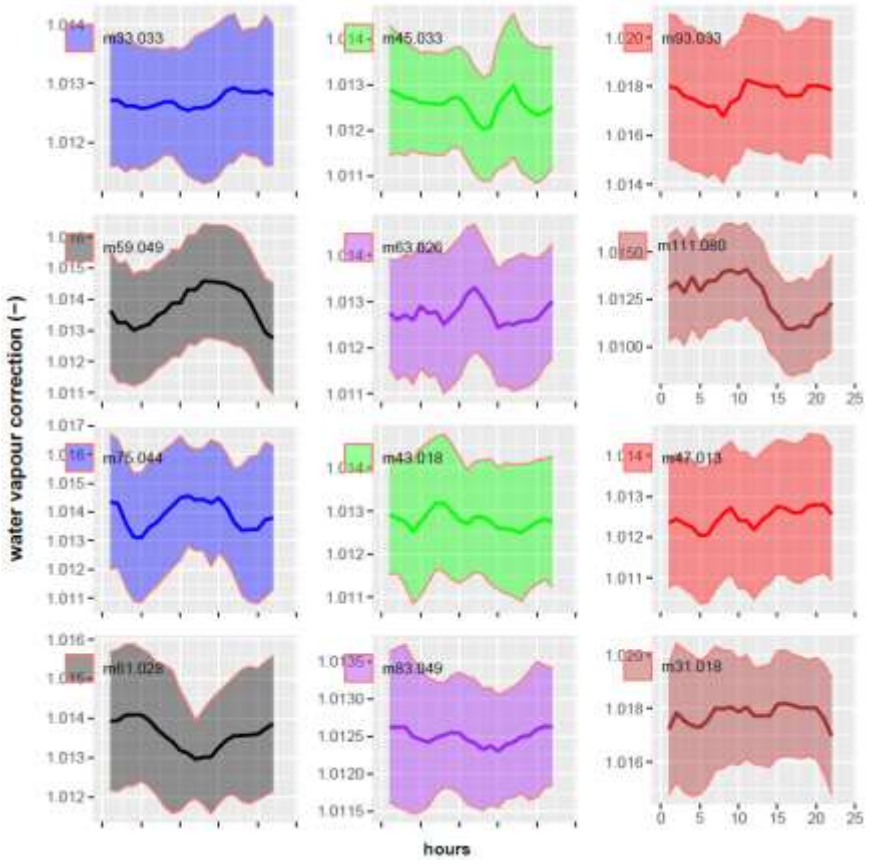

Figure S1. Example effect of water vapour dilution and fluctuations on the fluxes of the 6 most emitted and 6 most deposited VOCs.

5.2 Effect of ion source normalisation in eddy-covariance fluxes computation

An additional issue when using a PTRMS to measure fluxes by eddy-covariances, is the fact that the primary ion from the source (H_3O^+) is consumed by all compounds protonated and hence shows a fluctuation that is correlated with *w*. Usually in a PTRMS, the assumption is made that the consumption of H_3O^+ ions in the drift chamber is limited (lower than 10% of produced H_3O^+) which hence allows to assume pseudo first order chemical reaction rates (Holzinger et al., 2019). Although this assumption holds in most conditions, the issue is somewhat different when looking at fluctuations (and not mean quantities). In particular, in the mixing ratios computations (eq. 1 to 3), there is a "normalisation" step that involves dividing by $cps^{trans}_{H_3O^+} + cps^{trans}_{H_2O.H_3O^+}$. The question arises whether this normalisation should be done on the raw data prior to covariance calculation or on the computed covariances. To the best of our knowledge, this question has not been addressed before. To answer this question, we differentiate eqns. (1 - 4) and combine them with eq. (S9). In the differentiation process, we have considered all terms, except counts per seconds (cps), to be constant, which is justified by the assumption that they should not be correlated with *w* and will hence disappear when introduced in eq. (S9). We eventually find:

$$\chi'_i = S_i \times \chi_{i,ptr} \times \left\{ \frac{cps'_{R_iH^+}}{cps_{R_iH^+}} - \frac{\left(cps'_{H_3O^+} + \frac{TR_{H_3O^+}}{TR_{H_2O.H_3O^+}} cps'_{H_2O.H_3O^+} \right)}{\left(cps^{trans}_{H_3O^+} + cps^{trans}_{H_2O.H_3O^+} \right)} \right\} \quad \text{(S10)}$$

Incorporating eq. (S10) into eq. (S9), simplifying the notation $cps_{\mathrm{i}} = cps_{\mathrm{R_iH^+}}$, and $tr_v = \frac{\mathrm{TR}_{\mathrm{H_3O^+}}}{\mathrm{TR}_{H_2O.\mathrm{H_3O^+}}}$, one gets:

$$F_i = S_i \overline{\left(\frac{\chi_{\iota,ptr}}{cps_{\mathrm{i}}}\right)} \left(\overline{w' cps'_{\mathrm{i}}} - \frac{cps_{\mathrm{i}}}{cps^{trans}_{\mathrm{H_3O^+}} + cps^{trans}_{H_2O.\mathrm{H_3O^+}}} \overline{w' \left(cps'_{\mathrm{H_3O^+}} + tr_v \, cps'_{H_2O.\mathrm{H_3O^+}} \right)} \right) \times \frac{\overline{p_a{}^d}}{R\overline{T_a}} \times \left(1 + \frac{p_{vap}}{p_a} + \frac{1}{V_{exch,i}} \cdot \frac{E}{M_v} \frac{RT_a}{p_{,a}} \right) \quad \text{(S11)}$$

The normalisation factor here is $\overline{\chi_{\iota,ptr}/cps_{\mathrm{i}}}$, which, based on eqns. (1) and (2) can be expressed as follows:

$$\overline{\chi_{\iota,ptr}/cps_{\mathrm{i}}} = 1.657\, e^{-11} \times \frac{\mathrm{U_{drift}\, T^2_{drift}}}{\mathrm{k\, p^2_{drift}}} \times \frac{\mathrm{TR}_{\mathrm{H_3O^+}}}{\mathrm{TR}_{\mathrm{R_iH^+}}} \left(\frac{1}{\overline{cps^{trans}_{\mathrm{H_3O^+}} + cps^{trans}_{H_2O.\mathrm{H_3O^+}}}} \right) \quad \text{(S12)}$$

In practice, when computing the flux, if the covariance is calculated on non-normalised cps, the term including $cps'_{\mathrm{H_3O^+}} + tr_v \, cps'_{H_2O.\mathrm{H_3O^+}}$ in eq. (S11) is not taken into account and the normalisation is simply done with the normalisation factor in eq. (S12). If the cps are normalised prior to the covariance calculation, then an additional term in eq. (S11) appears that is mostly negative. Indeed, $cps'_{\mathrm{H_3O^+}} \gg tr_v \, cps'_{H_2O.\mathrm{H_3O^+}}$ and $\overline{w' \, cps'_{\mathrm{H_3O^+}}}$ is usually negative because the sum of VOCs and water emissions are usually larger than deposition and hence $cps'_{\mathrm{H_3O^+}}$ is inversely proportional to the sum of VOCs and water (it is consumed by reaction these compounds). This term can be rearranged to show up the biased and unbiased flux:

$$F_i^{biassed} = F_i^{unbiassed}(1 - A) \quad \text{(S13)}$$

Where:

$$A = \frac{cps_{\mathrm{i}}}{cps^{trans}_{\mathrm{H_3O^+}} + cps^{trans}_{H_2O.\mathrm{H_3O^+}}} \frac{\overline{w' \left(cps'_{\mathrm{H_3O^+}} + tr_v \, cps'_{H_2O.\mathrm{H_3O^+}} \right)}}{\overline{w' cps'_{\mathrm{i}}}} \quad \text{(S14)}$$

In Figure S2 we have evaluated the magnitude of this additional term by comparing the fluxes calculated by normalising before and after covariance computation. We see that this has little effect on the methanol flux (less than a few %) except during some nights. This is explain by the fact that the covariance $\overline{w' \, cps'_{\mathrm{H_3O^+}}}$ is multiplied by a factor that is inversely proportional to the ion source strength and is hence very small (lower than 3.10^{-3}). Hence, even if it is 10 times the compound flux, it remain small.

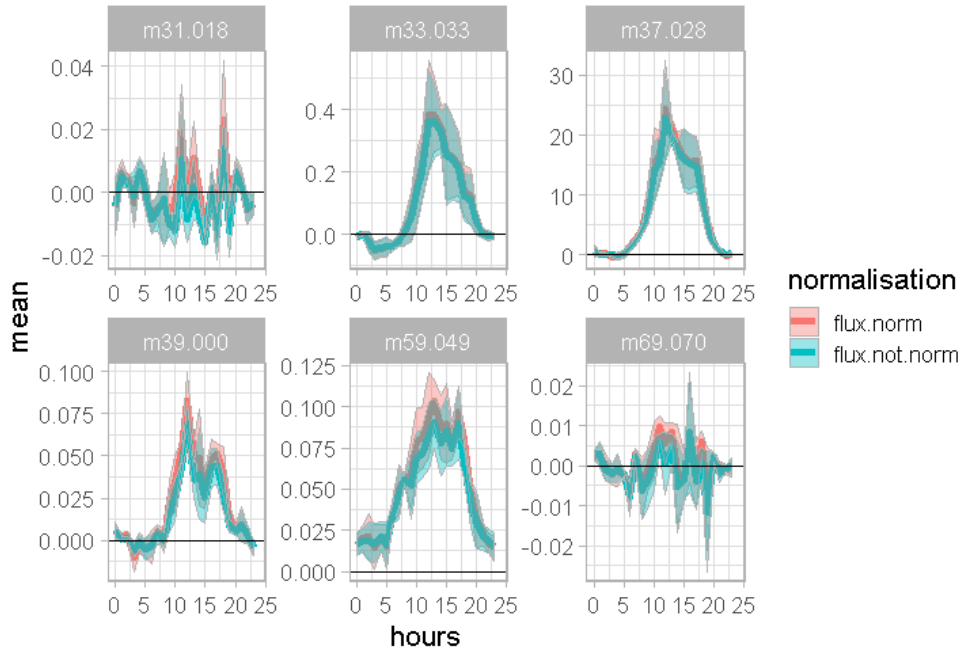

Figure S2. Example effect of cps normalisation on the fluxes of some key compounds. Red curves (flux.norm correspond to flux calculated using normalised cps, while blue curves (flux.not.norm) correspond to fluxes calculated using raw cps.

In Figure S3, we show the term $(1 - A)$, which is the ratio of biased to unbiased flux, averaged over the whole period. It shows that the averaged bias is lower than 10% either positive (methanol, acetaldehyde) or negative (acetone). The bias is only large during the night and can vary between situations (interquartile up to 20%), but is most of the time lower than a few percents.

The main finding here is therefore that when normalisation is performed on a raw signal, an additional term should be taken into account but it seems to be in general quite small. On the contrary, if normalisation is performed after calculating the covariance on cps_i raw signals no additional term needs to be taken into account. In this study, we therefore chose to perform normalisation after covariance computation at a 5 min time step.

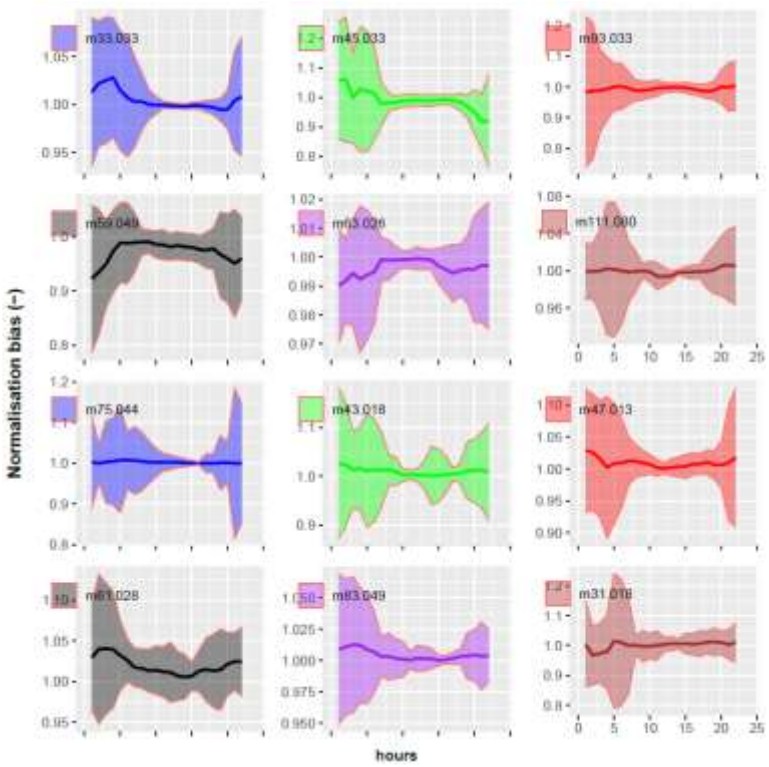

Figure S3. Bias introduced by normalising the cps by the primary ion prior to calculating the covariance, for the 6 most emitted and 6 most deposited compounds. Term (1-*A*) in equation (S13).

6 Lag decorrelation time and high frequency losses corrections

The decorrelation time lag was determined as the maximum of the correlation function between the vertical component of the wind speed and the component mixing ratio (or temperature). It can be seen from the example in **Figure S4** that the correlation functions for the instruments positioned at the end of the sampling line had a ~2.5 s delay and that the shapes of the correlation functions are very similar between air temperature (Ta) and mixing ratios from the QCL and the PTRMS. The PTRMS has a somewhat shorter lag time than the QCL, which can be explained by the smaller tube diameter and length between the main sampling line and the PTRMS subsampling, as well as the lower drift tube volume, compared to sampling system and optical cell of the QCL.

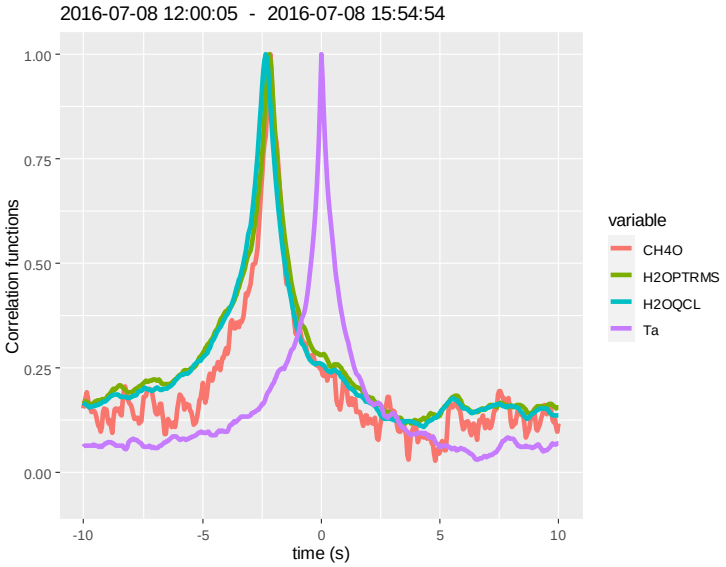

Figure S4. Example correlation functions between vertical component of the wind speed, sonic air temperature (Ta), the water vapour mixing ratio measured the QCL (H2OQCL) and the first H_2O cluster ion (H2OPTRMS). Data from 8 July from 12 to 16 hours UTC..

High frequency losses is an issue when measuring a flux using a long sampling line. The conditions chosen in this experiment ensured a short lag time as shown in **Figure S4**, suggesting high frequency losses should be small. Evaluation of these with the theoretical approach of Massman et al. (1991) provides an estimate of around 5% attenuation. However, in-situ measurements are more powerful for obtaining real conditions attenuations. The cross-spectra for the QCL water vapour and the PTRMS first water cluster were therefore computed and compared to the temperature cross-spectra (**Figure S5**). Water vapour proxy was used, since for other VOC, the cross-spectra was too noisy to compute a high frequency loss. We computed from co-ogives that high frequency losses represented less than a few percent of the flux for the water vapour cluster (Ammann et al., 2006). Usually, the QCL water vapour measurement showed higher HF losses than the first water cluster measured by the PTRMS, which is consistent with the slightly higher lag time observed in **Figure S4**.

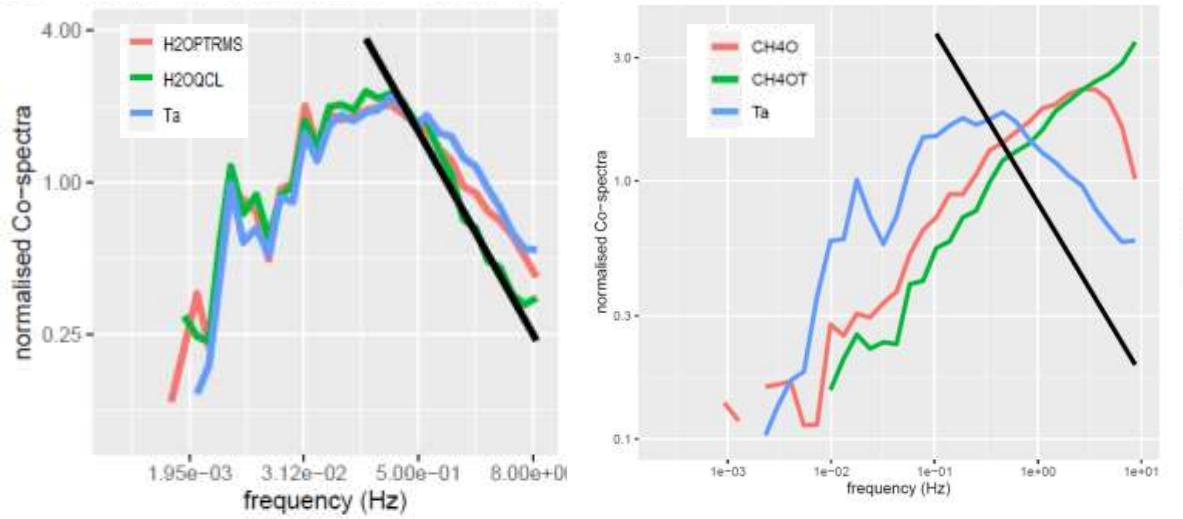

Figure S5. Normalised cross-spectra multiplied by the frequency. Shown are the cross spectrum between vertical component of the wind speed (W), sonic air temperature (Ta), the water vapour mixing ratio measured the QCL (H2OQCL), the first H_2O cluster ion (H2OPTRMS), the methanol (CH4O) and a mimic of the methanol signal based on the temperature signal plus noise (CH4OT). The cross spectra have been normalised by their mean values. Data from 8 July from 12 to 16 hours UTC. The black line shows the expected decrease in co-spectra for high frequencies based on the Monin Obukohv energy cascade theory (CoSP ~ $f^{-3/2}$). The CH4OT signal was computed as the temperature signal centred and normalised by the variances of methanol to temperature on which was added a white noise of mean and standard deviation equal to that of methanol.

7 Meteorological conditions and O_3 and NO_x mixing ratios

This section shows graphs of the meteorological conditions.

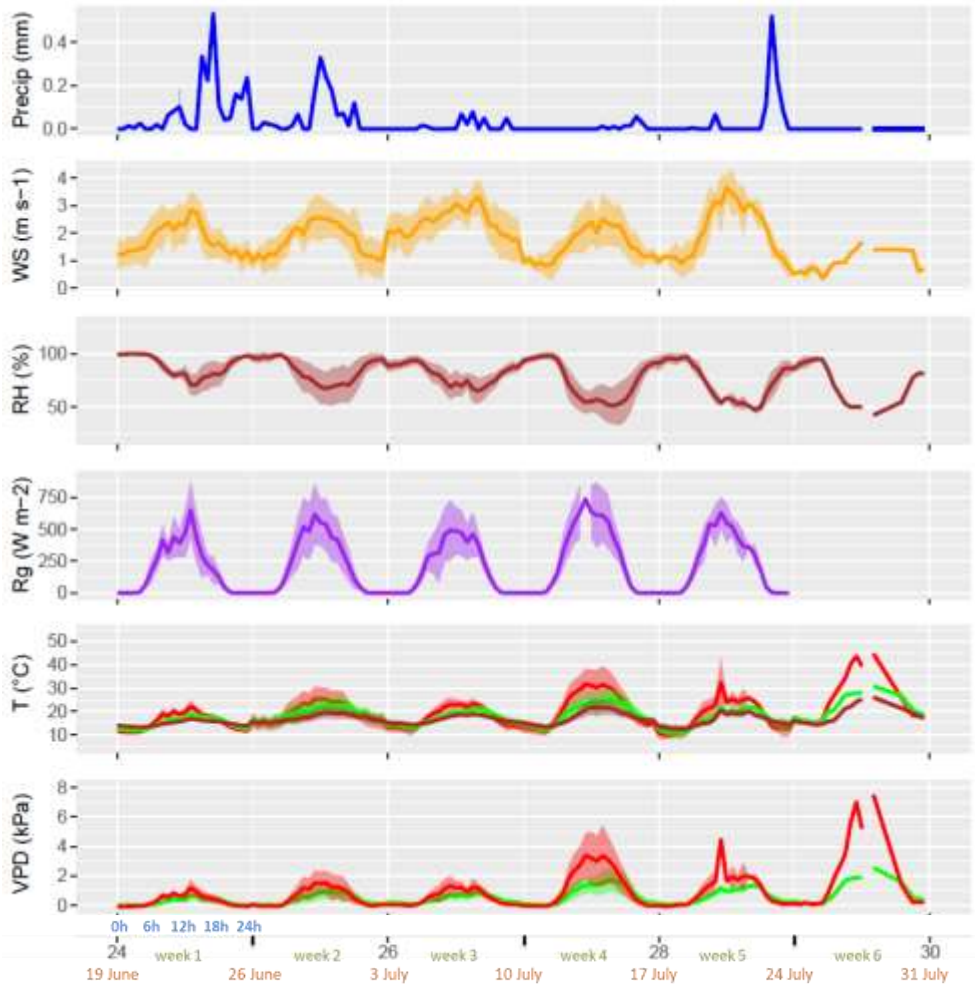

Figure S6. Meteorological conditions at the site during the experiment at the reference height measured by eth ICOS FR-GRI station. Precipitation (P), wind speed (WS), relative humidity (RH), solar incoming radiation (Rg), air (green), crop (red) and soil (5 cm depth, brown) temperatures, vapour pressure deficit of the air (green) and the leaf surface vapour pressure deficit VPD(Tz0, red), and dew occurrence potential (dew) as estimated with negative periods of VPD(Tz0). Each week shows the diel cycle with its mean (line) and standard deviation (ribbons). The x-axis shows the week number in the year (black) and over the experiment (green), starting date of the week (orange), hour of day (blue).

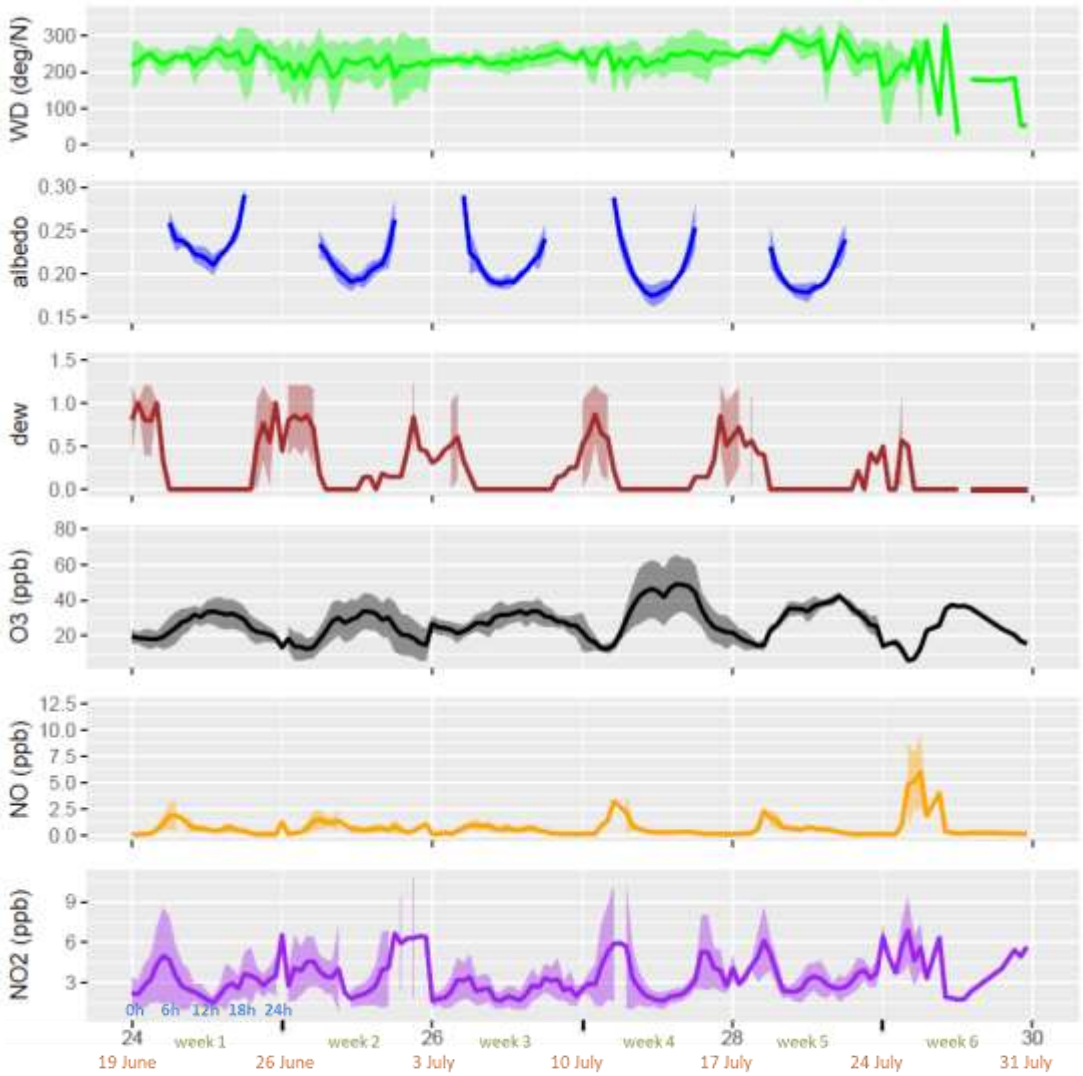

Figure S6. Meteorological conditions, continued. Wind direction (WD), albedo, wetness index (dew, 1 = surfaces fully covered by water, 0 = dry surfaces), and O_3, NO and NO_2 mixing ratios. Each week shows the diel cycle with its mean (line) and standard deviation (ribbons). The x-axis shows the week number in the year (black) and over the experiment (green), starting date of the week (orange), hour of day (blue).

8 VOC mixing ratio

This section provides the graphs of VOC mixing ratios

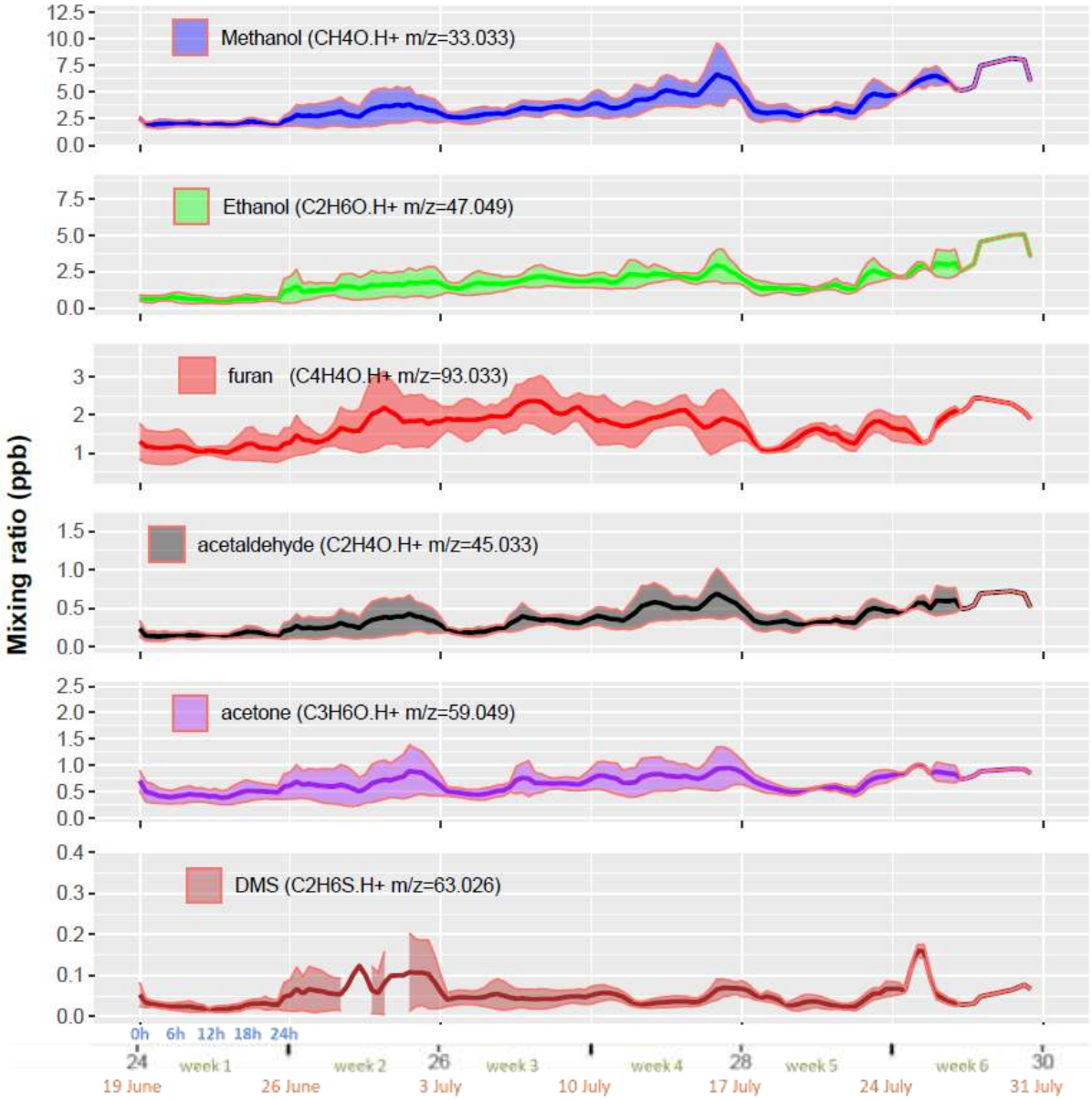

195 **Figure S7a. Mixing ratios at 2.7 m above ground of the six most emitted VOC. Each week shows the diel cycle with its mean (line) and standard deviation (ribbons). The x-axis shows the week number in the year (black), the week number in the experiment (green), the starting date of the week (orange), and the hour of day (blue).**

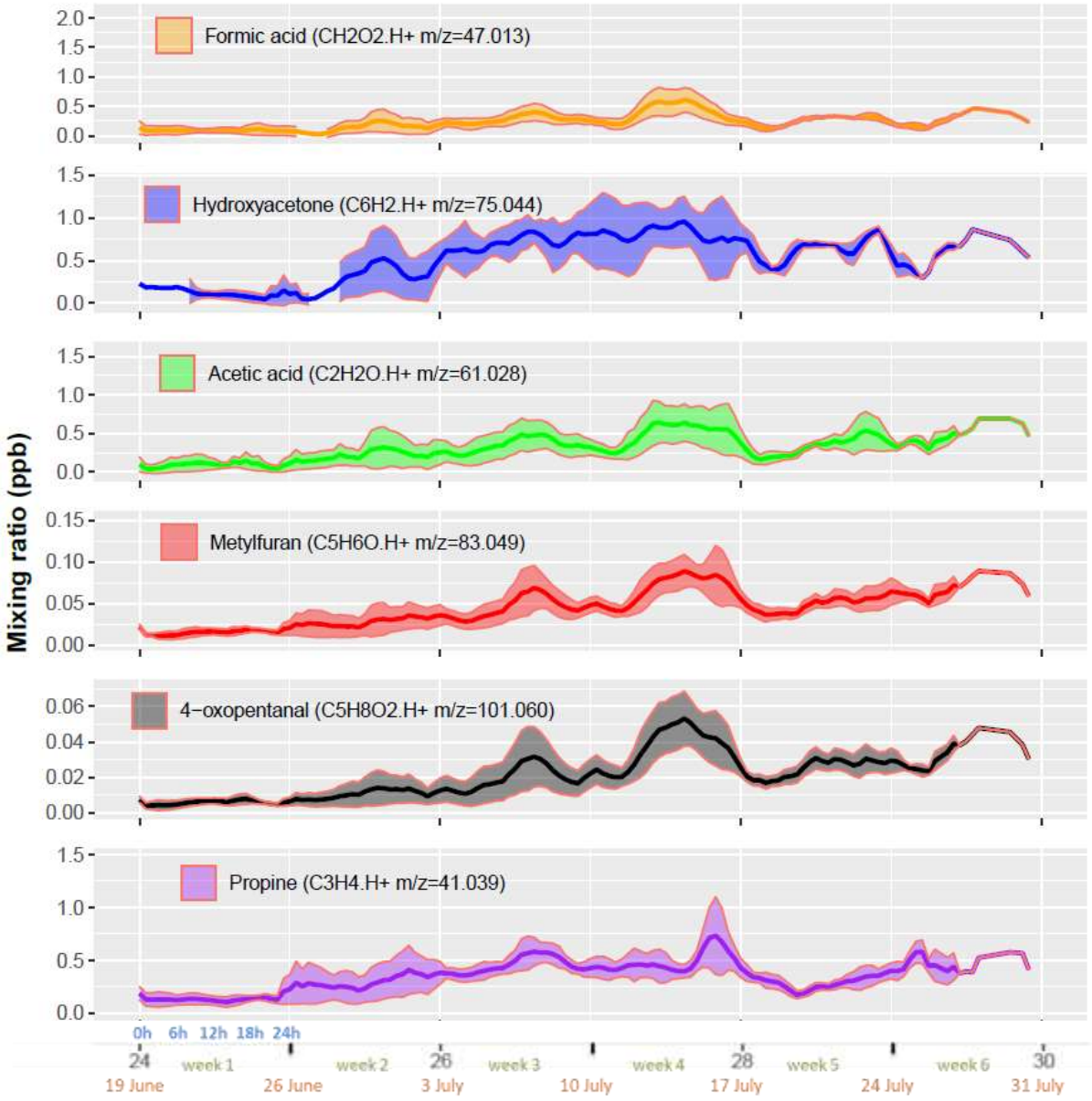

200 **Figure S7b. Mixing ratios at 2.7 m above ground of the six most deposited VOC. Each week shows the diel cycle with its mean (line) and standard deviation (ribbons). The x-axis shows the week number in the year (black), the week number in the experiment (green), the starting date of the week (orange), and the hour of day (blue).**

9 Water vapour mixing ratios and fluxes as measured by the PTR-Qi-TOF-MS

Comparison of water vapour mixing ratios and fluxes measured by the IRGA and the PTR-Qi-TOF-MS water clusters (m/z 37.028, m/Z 55.039) allows estimating the capability of the instrument to measure water vapour fluxes and thereby giving confidence in VOC measurements. The comparison of the mixing ratios (**Figure S8**) shows that the water cluster mixing ratios were not stably correlated to atmospheric water vapour. Moreover, the water clusters seem to be poor proxies of the atmospheric water vapour pressure over the entire period.

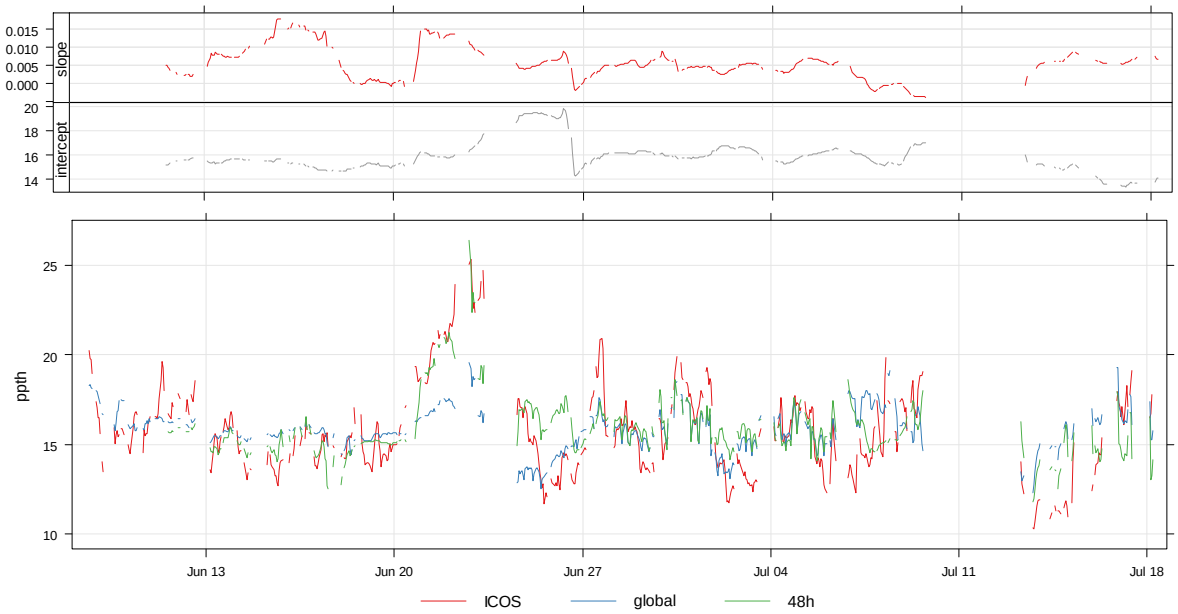

Figure S8. Water vapour mixing ratios as measured from IRGA (ICOS), and the PTR-Qi-TOF-MS either calibrated over the entire period or over rolling 48 h.

On the contrary, the comparison of water vapour fluxes as retrieved with an IRGA and the PTR-Qi-TOF-MS water clusters (**Figure S9**) shows a better agreement indicating that the water vapour cluster fluctuations in the PTR-Qi-TOF-MS are correlated to the atmospheric water vapour fluctuations, and hence suggesting that the offset of the PTR-Qi-TOF-MS water cluster may be fluctuating. We can conclude that the PTR-Qi-TOF-MS should be used with cautious to estimate the water vapour fluxes and can hardly be used to measure the water vapour mixing ratios.

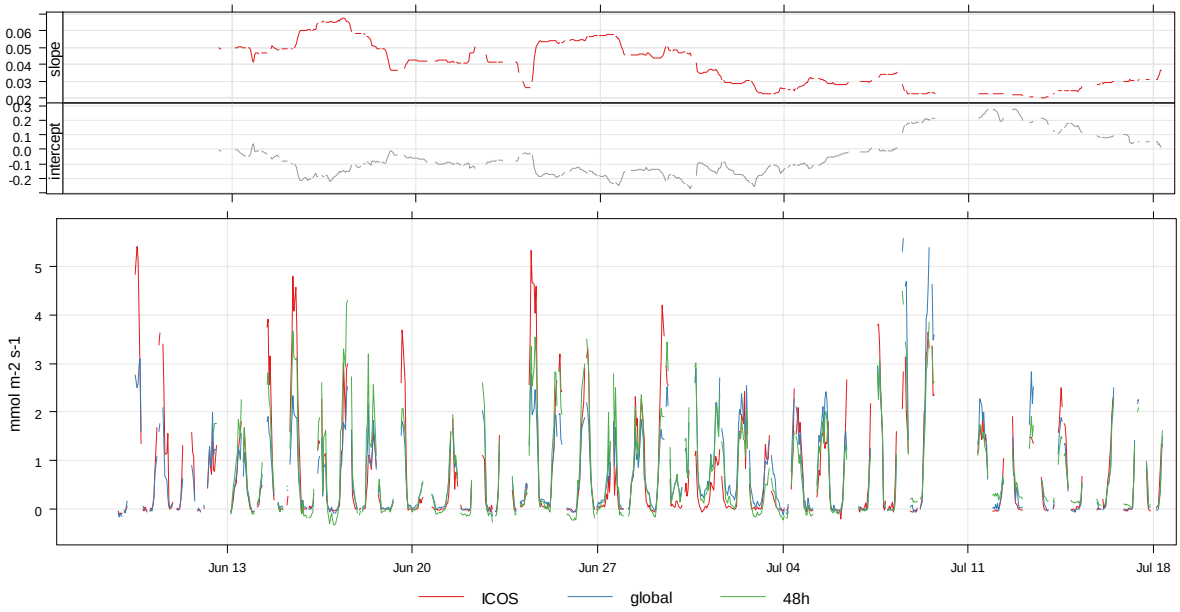

Figure S9. Bottom graph: water vapour flux as measured at ICOS, and the PTRMS either calibrated over the entire period or over rolling 48 h. The slope and intercepts of the rolling calibration are also given in the top graph.

10 Evaluating the capability of the PTR-Qi-TOF-MS to measure CO_2 fluxes and mixing ratios

The $CO_2.H^+$ channel (m/z 44.99) may be thought to be used for estimating the CO_2 mixing ratio with PTR-Qi-TOF-MS. However, since CO_2 has a proton affinity much lower than H_2O, $CO_2.H^+$ is likely produced out of the drift tube in the electromagnetic lenses, and may not be a good proxy of the atmospheric CO_2. It is therefore interesting to check if it is representative of the ambient CO_2 mixing ratios. **Figure S8** clearly shows that the $CO_2.H^+$ signal cannot be representative of the CO_2 flux over the period, since daily CO_2 flux changes from negative to positive values with the canopy senescence while the $CO_2.H^+$ flux remains negative all the time. Hence, we can conclude that $CO_2.H^+$ should not be used as a CO_2 proxy, unless proven by laboratory calibrations.

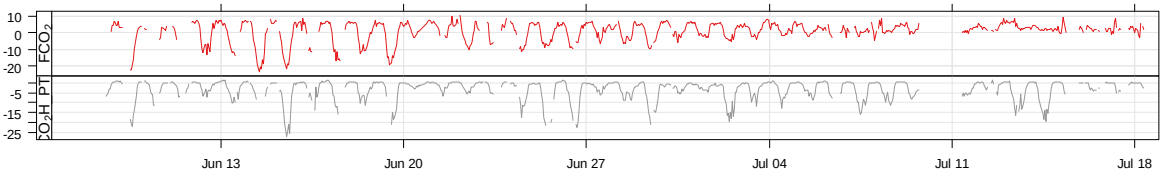

Figure S10. Comparison of the CO2 flux measured by the IRGA and the CO2.H+ flux measured by the PTRMS.

11 Fragmentations to and from mass m/z 69.070 in relation with E/N

It is well known that some VOC (like MBO, 2-methyl-3-buten-2-ol, $C_5H_{10}O$, m/z 87.080) fragment to m/z 69.07 and that the fragmentation pattern may be dependent on E/N (Zhou et al., 2017;Bachy et al., 2020). It is also known that m/z 69.07 fragment to lighter ions (41.039, 57.070). In this study, E/N changed over the course of the experiment from 150 to 130, giving the opportunity to check its effect on the fragmentation of m/z 69.07 fragments

present on m/z 69.07. Karl et al. (2012) showed that isoprene and MBO could be separated by using NO^+ ionisation, which produces the ion m/z 68.062 ($C_5H_8^+$). Since our PTRMS produces also a small quantity of NO^+, but also O_2^+, which would lead to the same ionisation of isoprene to m/z 68.062, we tracked m/z 68.062 and found a high correlation between mixing ratios at m/z 68.050 and m/z 69.070 with E/N 150 (spearman correlation 0.97), which was a bit lower with E/N 130 (0.92), suggesting that heavier ions may be fragmenting at at m/z 69.070. At E/N = 150, m/z 69.070 was also highly correlated with ions m/z 41.039 (corr. 0.97) and 57.070 (corr. 0.98), as expected. At E/N = 130, the correlations with these ions are lower, suggesting less fragmentation of isoprene to these ions at that E/N state. **Figure S9** shows that m/z 68.062, when scaled up by the slope of the regression between 69.07 and 68.062 obtained for E/N = 150 follows well the m/z 69.07 during the period with E/N=150. When multiplied by the same slope obtained for E/N=130, we have an upper estimation of the m/z 69.070 value at E/N=150. This suggests indeed that almost half of the m/z 69.070 was fragmented for E/N 150.

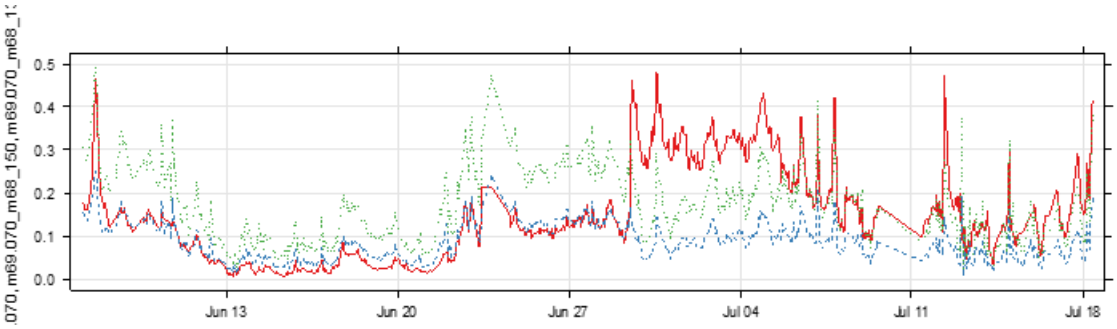

Figure S11. Time course of m/z 69.070 (red) and m/z68.049*12.3 (blue) mixing ratios over the course of the experiment. E/N changed from 150 before the 29 June to 130 afterwards

12 Wind roses analysis

Figure S12 shows wind roses of methane, NO and N_2O measured at the site. Methane shows the typical wind rose for compounds emitted by the farm, since it is a good tracer of farm emissions. On the opposite, NO is a good tracer of the traffic contribution from the nearby road and the city of Paris on the west. Finally, N_2O shows a quite undetermined wind rose which is expected.

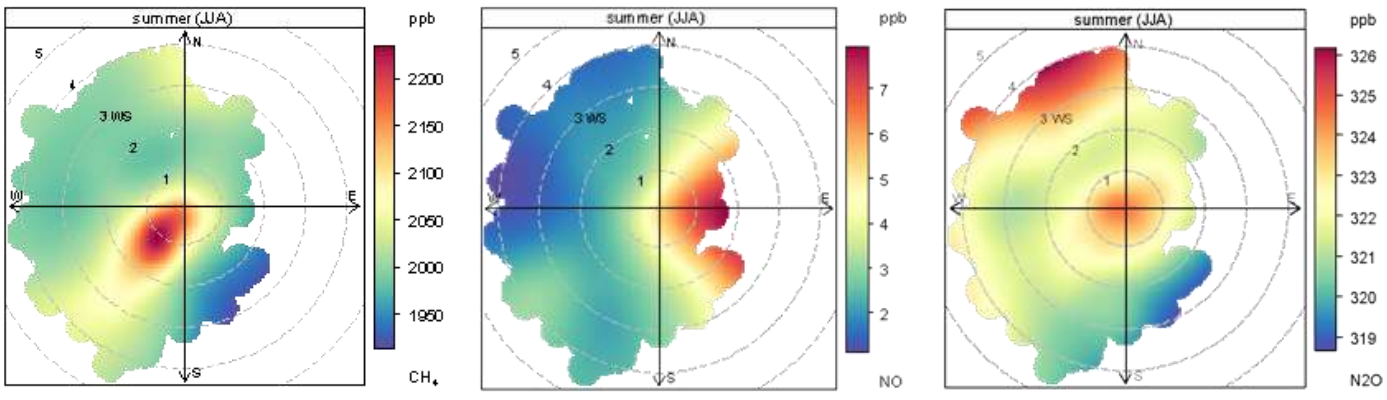

Figure S12. Pollution roses for CH4, NO and N2O.

Figure S13 shows the wind roses for all the VOC compounds that were identified as coming from the farm. We clearly see an increase in the normalised mixing ratio from the Farm wind sector (~200 deg/N). Some ion peaks belong to the same original ion and were not filtered out for this figure (See **Table S2a for correlations**)

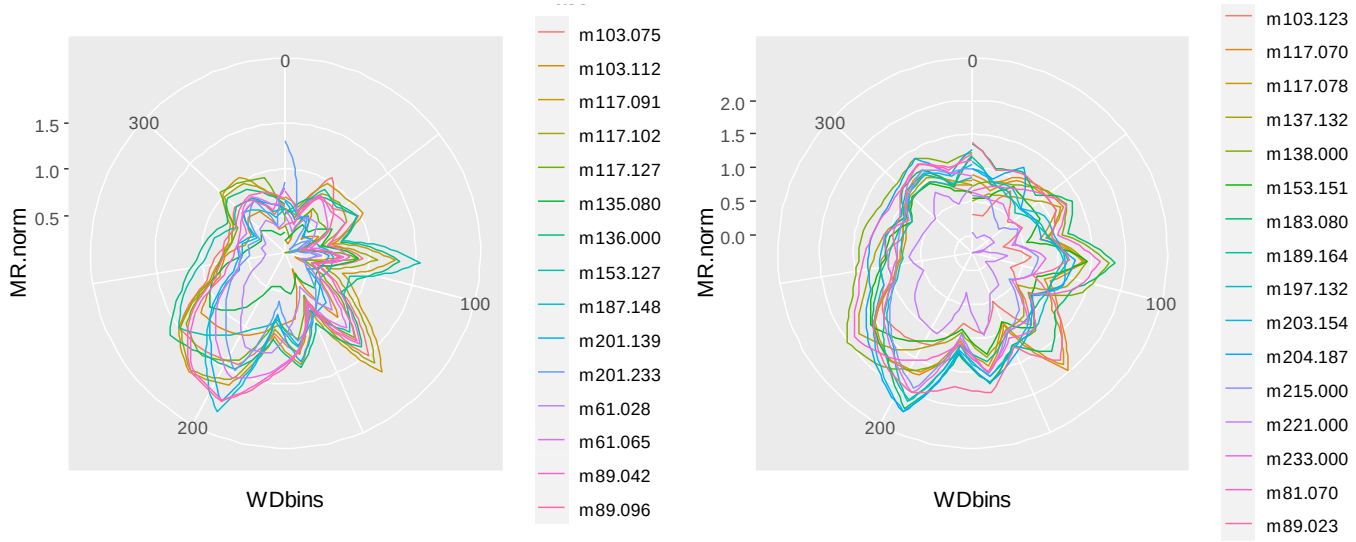

Figure S13. Wind roses of normalised mixing ratios showing an increase when wind is blowing from farm. Normalisation is achieved by dividing the mixing ratio by its standard deviation.

Figure S14 shows the averaged mixing ratio as a function of the average air temperature by separating the farm wind sector and the other wind sectors. We see that for some compounds the difference between Farm sector and the other sector show an optimum temperature around 20°C-25°C, suggesting a biological or chemical optimum process.

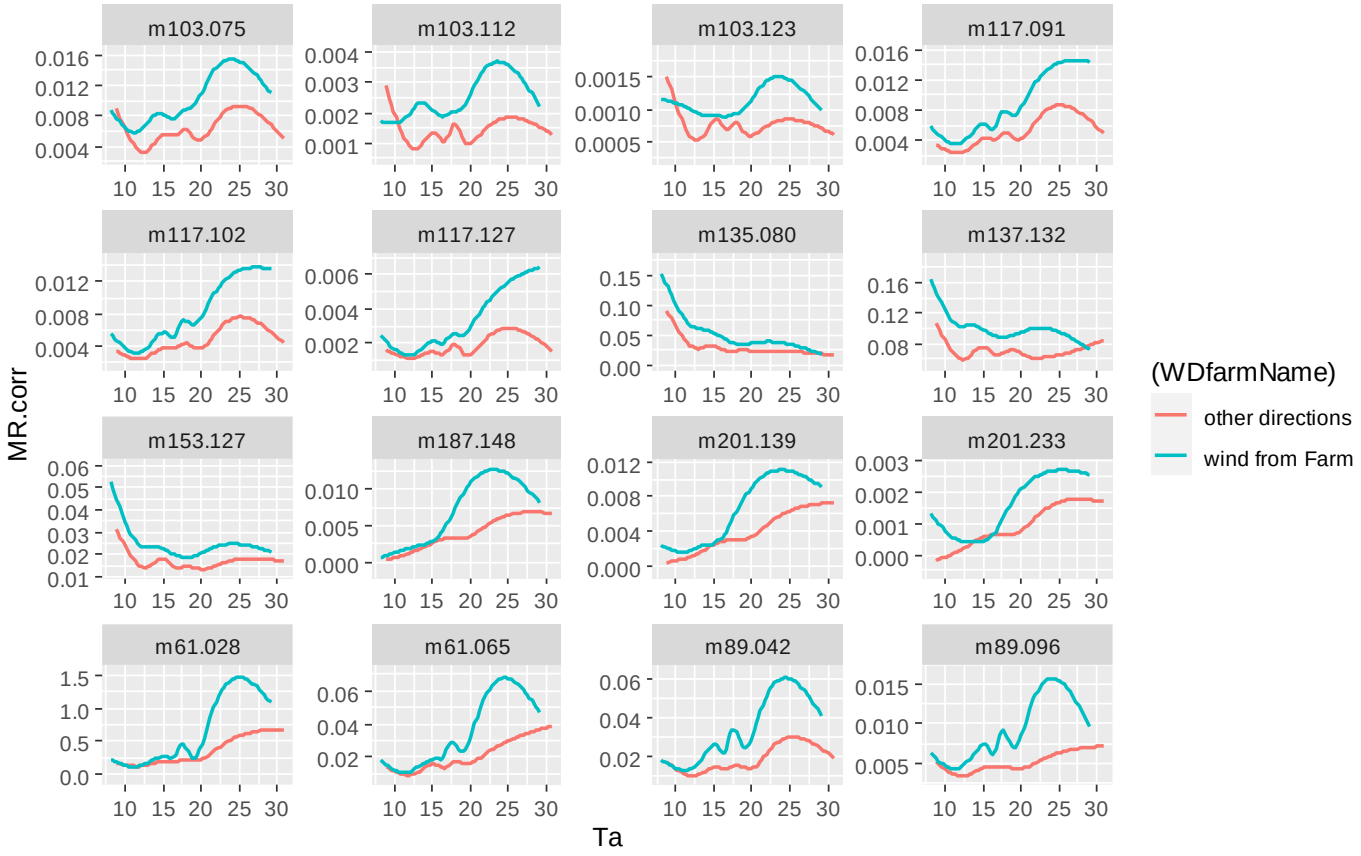

Figure S14. Mixing ratios of compounds identified as coming from the farm, as a function of air temperature.

13 Ratio of acetone to methanol mixing ratios at the site

Acetone to methanol mixing ratios is a quantity measured in many atmospheric chemistry studies. **Figure S15** shows this ratio over the course of the experiment.

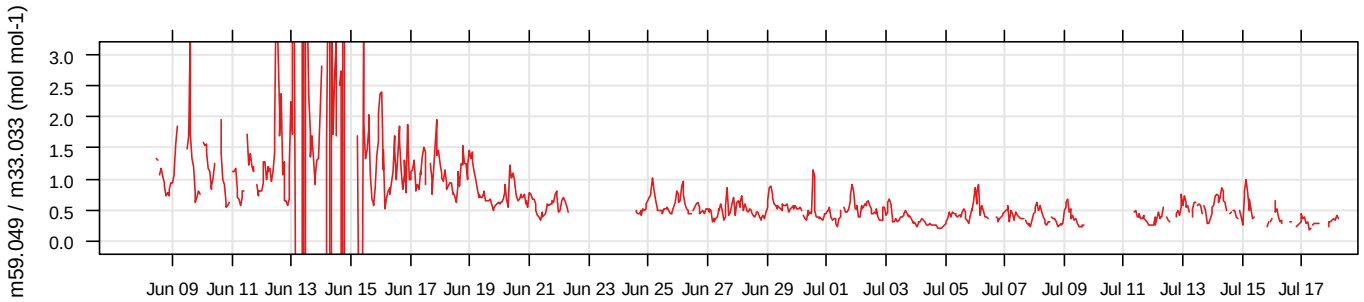

Figure S15. Ratio of acetone to methanol mixing ratios at 2.7 m above the ground as a function of time.

14 Flux limit of detection (LOD)f.

The flux limit of detection was computed following the methodology of Wienhold (1994). **Figure S17** shows LODf and averaged fluxes for all ions that matches the condition that the flux is larger than 3 times the overall LOD. The hourly averaged LODf is much higher since it does not integrated over the large number of samples collected during the experiment (see computation details in the text).

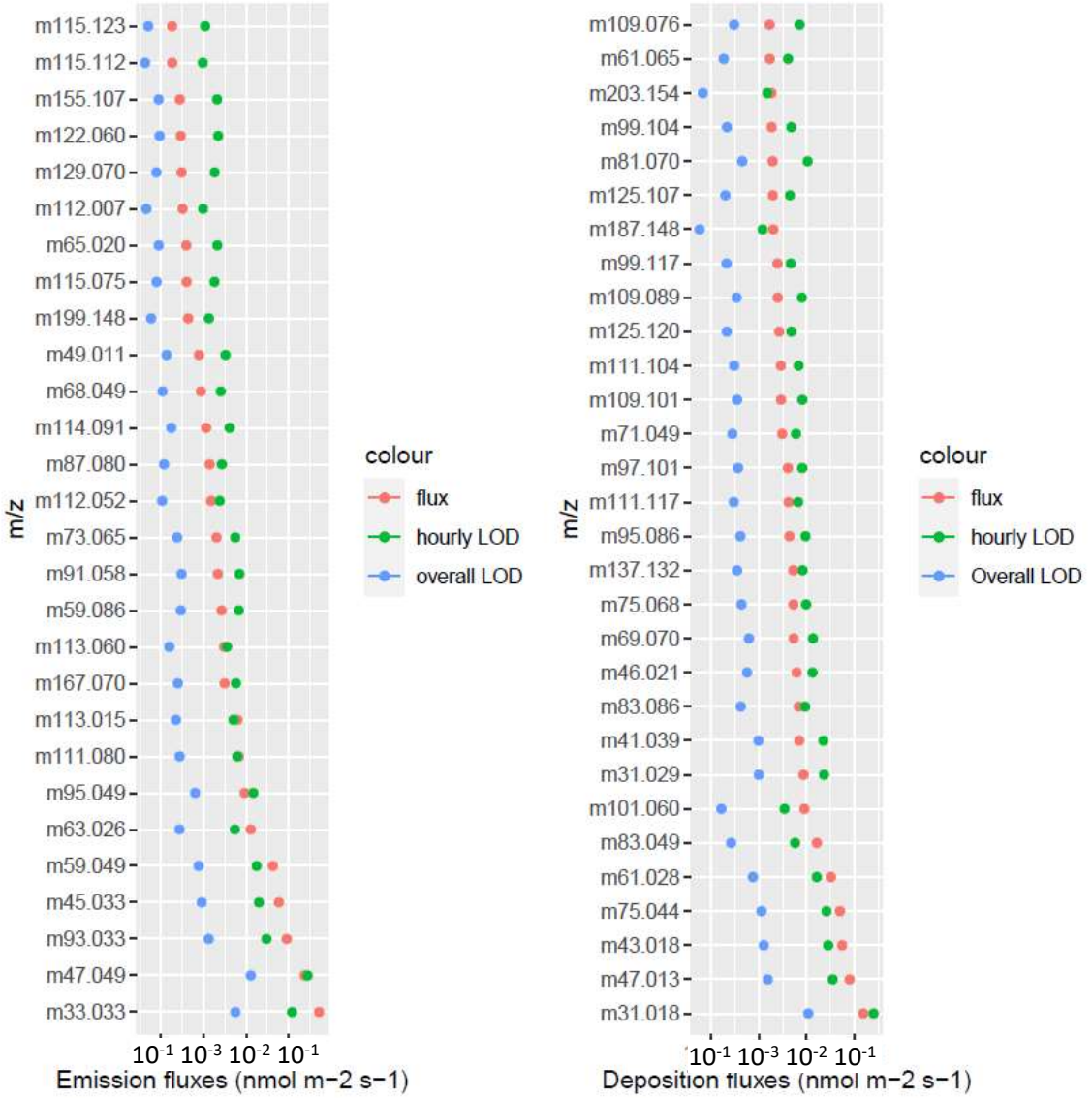

Figure S16. Mean fluxes and LODf of 30 most emitted (left) and most deposited (right) ions over the entire period. Hourly averaged LODf and LODf computed over the whole period are shown.

15 Non-VOC species mixing ratios

15.1 Ozone and nitrogen oxides monitoring

Ozone (O_3), and nitrogen oxides (NO and NO_2) were monitored at the reference height with the same line as the Eddy-Covariance. Air was subsampled through a Teflon pump (KNF 840.FT.18) from a flow rate in excess of 5 L min^{-1} to the analyser sample flow rates. Tubes were heated to 60°C. A chemiluminescence analyser (42C, ThermoEnvironment, USA) was used for NO and NO_2, and a UV absorption spectrometry analyser (49i, ThermoEnvironment, USA) was used for O_3. The analysers were logged by the same Labview application at 20 Hz and averaged at 5 min. The NO/NO_2 and O_3 analysers were calibrated using a gas phase titration (GPT) unit (SX6000, LNI, SW) with a high quality grade zero air cylinder (99.9999%, Air Liquide, FR) and a 20 ppm NO cylinder (high grade, Air liquide, FR). Zero and 80 ppb of NO were generated for NO calibration. For NO_2 and O_3, a prescribed concentration of O_3 was added in the GPT stream which induced a decrease of NO that corresponded to the amount of O_3 that reacted with NO and was used to calibrate the NO_2 and O_3. The calibration uncertainty was evaluated as 2% for NO_x and 3% for O_3.

15.2 Evolution of the non-VOC mixing ratios over time

The CO_2 mixing ratios varied from 363 to 526 ppm and showed a typical daily pattern for a measurement over a crop with largest values at night when the respiration was large and mixing was low, and lowest values during the day when absorption and mixing were both large (**Figure S17**). The slowing down of the crop photosynthesis was characterised by the increase of the daily minimum CO_2 mixing ratios, while large night-time values observed towards the end of the campaign rather translate stable atmospheric conditions. During windy nights CO_2 mixing ratio remained low due to good mixing of the boundary layer. Water vapour mixing ratios varied quite a lot from 10 to 25 ppth and showed an increase during 20-25 June following the main precipitation event and were the lowest the 11-14 July. There was no clear daily pattern of water vapour mixing ratios, indicating, as expected, that the daily pattern in RH was mostly related to temperature change (**Figure S6**).

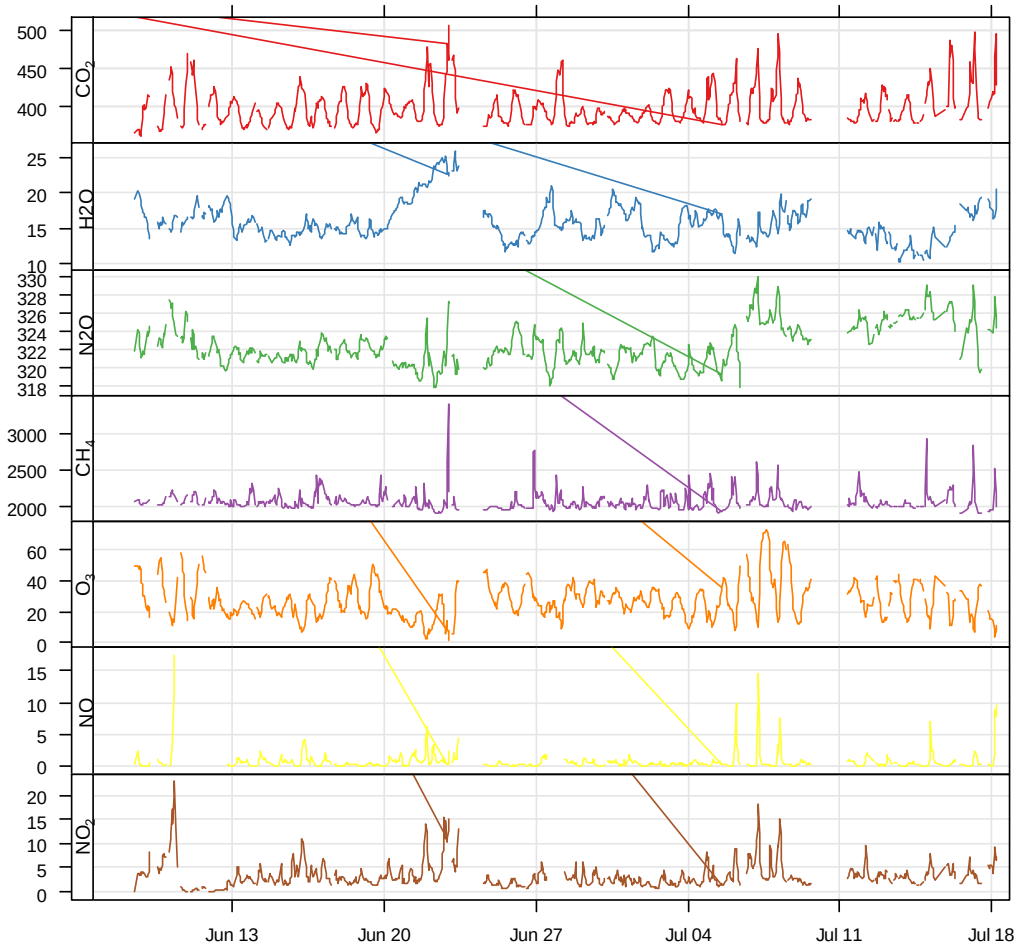

Figure S17. Mixing ratios of CO_2 (ppm) , H_2O (ppth), CH_4 (ppb), O_3 (ppb), NO (ppb)and NO_2 (ppb).

The CH_4 mixing ratio varied from 1907 to 3402 ppb and showed a slight daily pattern similar to CO_2 but with very marked peaks that occur mostly during nights and can be attributed to advection of methane from the nearby dairy farm as clearly showed in **Figure S12**. The ozone mixing ratio varied from 1.5 to 73 ppb and showed a marked daily pattern with daily maximum occurring in the afternoon and night time minimums. The largest concentrations occurred during the warmest periods in early June and July which also corresponded to peaks in NO and NO_2 mixing ratios generated by regional traffic peaks due to the summer holidays rush. NO varied from 0.01 to 17 ppb and peaked at rush hours and during calm nights. An increase was also observed during the slightly rainy period (13-25 June) which may be due to local NO emissions from soils. The NO_2 mixing ratio varied from 0 to 23 ppb and mostly increased in air masses coming from Paris, which also corresponds to the flux footprint being the lowest (east-north-east).

16 Isoprene and Monoterpenes fluxes

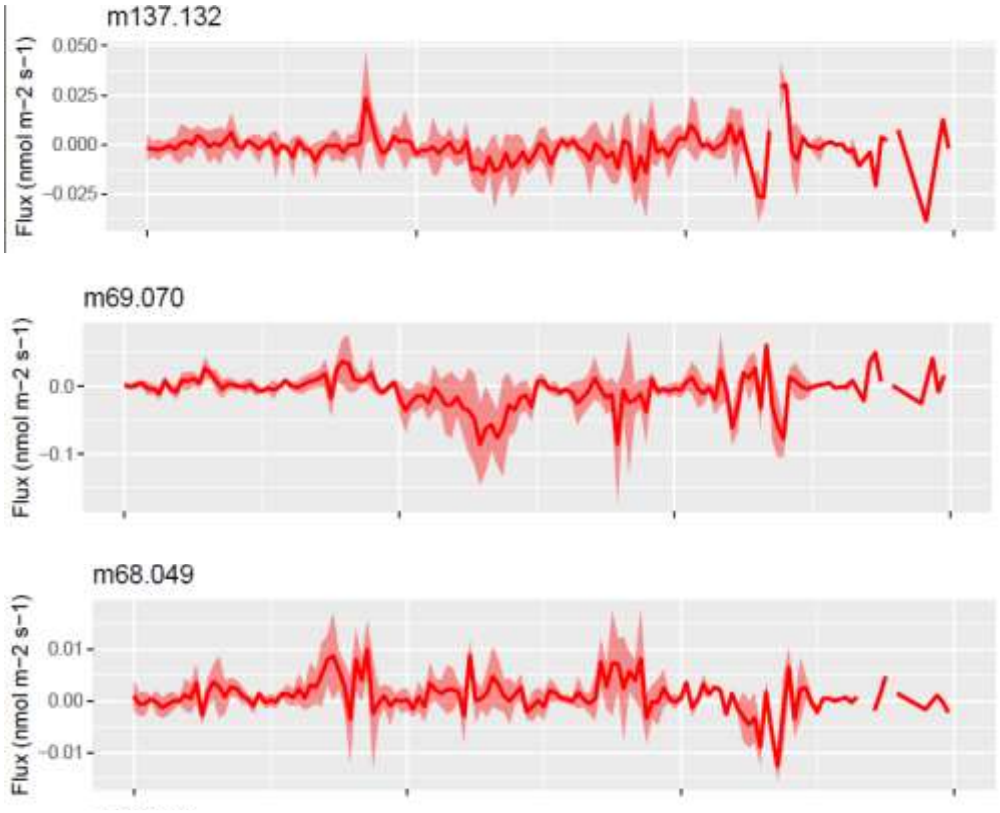

Figure S19. Fluxes of isoprene and monoterpenes over the wheat canopy. The x-axis shows the week number. In each week, the diel cycle is shown with mean and standard deviation.

References

Ammann, c., brunner, a., spirig, c., and neftel, a.: technical note: water vapour concentration and flux measurements with ptr-ms, atmospheric chemistry and physics, 6, 4643-4651, doi 10.5194/acp-6-4643-2006, 2006.

Bachy, a., aubinet, m., amelynck, c., schoon, n., bodson, b., delaplace, p., de ligne, a., digrado, a., du jardin, p., fauconnier, m. L., mozaffar, a., muller, j. F., and heinesch, b.: dynamics and mechanisms of volatile organic compound exchanges in a winter wheat field, atmos. Environ., 221, 10.1016/j.atmosenv.2019.117105, 2020.

Holzinger, r., acton, w. J. F., bloss, w. J., breitenlechner, m., crilley, l. R., dusanter, s., gonin, m., gros, v., keutsch, f. N., kiendler-scharr, a., kramer, l. J., krechmer, j. E., languille, b., locoge, n., lopez-hilfiker, f., materić, d., moreno, s., nemitz, e., quéléver, l. L. J., sarda esteve, r., sauvage, s., schallhart, s., sommariva, r., tillmann, r., wedel, s., worton, d. R., xu, k., and zaytsev, a.: validity and limitations of simple reaction kinetics to calculate concentrations of organic compounds from ion counts in ptr-ms, atmos. Meas. Tech., 12, 6193-6208, 10.5194/amt-12-6193-2019, 2019.

Karl, t., hansel, a., cappellin, l., kaser, l., herdlinger-blatt, i., and jud, w.: selective measurements of isoprene and 2-methyl-3-buten-2-ol based on no+ ionization mass spectrometry, atmospheric chemistry and physics, 12, 11877-11884, 10.5194/acp-12-11877-2012, 2012.

Massman, w. J.: the attenuation of concentration fluctuations in turbulent-flow through a tube, j. Geophys. Res.-atmos., 96, 15269-15273, doi 10.1029/91jd01514, 1991.

Wienhold, f. G., frahm, h., and harris, g. W.: measurements of n2o fluxes from fertilized grassland using a fast-response tunable diode-laser spectrometer, j. Geophys. Res.-atmos., 99, 16557-16567, 10.1029/93jd03279, 1994.

Zhou, p. T., ganzeveld, l., taipale, d., rannik, u., rantala, p., rissanen, m. P., chen, d., and boy, m.: boreal forest bvoc exchange: emissions versus in-canopy sinks, atmospheric chemistry and physics, 17, 14309-14332, 10.5194/acp-17-14309-2017, 2017.